AIAA JOURNAL
Vol. 43, No. 3, March 2005

Active Control of Nonlinear Panel Flutter Under Yawed Supersonic Flow

Khaled Abdel-Motagaly*
Boeing Phantom Works, Seattle, Washington 98134
Xinyun Guo†
Old Dominion University, Norfolk, Virginia 23529
Bin Duan‡
Claritas, Inc., Arlington, Virginia 22209
and
Chuh Mei§
Old Dominion University, Norfolk, Virginia 23529

A coupled structural–electrical modal finite element formulation for composite panels with embedded piezoelectric sensors and actuators is presented for nonlinear panel flutter suppression under yawed supersonic flow. The first-order shear deformation theory for laminated composite plates, the von Kármán nonlinear strain–displacement relations for large deflection response, the linear piezoelectricity constitutive relations, and the first-order piston theory of aerodynamics are employed. Nonlinear equations of motion are derived by extending the three-node triangular Mindlin (MIN3) plate element. Additional electrical degrees of freedom are introduced to model piezoelectric sensors and actuators. The system equations of motion are transformed and reduced to a set of nonlinear equations in modal coordinates. Analysis results for the effect of arbitrary flow yaw angle on nonlinear supersonic panel flutter are presented. The results show that the flow yaw angle has a major effect on the panel limit-cycle oscillation amplitude and deflection shape. Two different control methods are investigated for the suppression of nonlinear panel flutter. The first method is the linear quadratic Gaussian controller. The second method is the nonlinear output controller comprised of a linear quadratic regulator and an extended Kalman filter nonlinear state estimator. Closed-loop criteria based on the norm of feedback control gain and on the norm of Kalman filter estimator gain are used to determine the optimal location of piezoelectric actuators and sensors at different flow yaw angles. Optimal sensor and actuator locations for a range of yaw angles are determined by grouping the optimal locations for different angles within the range. The results demonstrate the effectiveness of piezoelectric materials and of the nonlinear output controller in suppressing nonlinear flutter of isotropic and composite panels at different flow yaw angles.

Nomenclature

$[A]$, $[B]$, $[D]$, $[A_s]$	=	laminate extension, coupling, bending, and shear stiffness matrices
$[\boldsymbol{A}]$, $[\boldsymbol{B}]$, $[\boldsymbol{C}]$, $[\boldsymbol{D}]$	=	linear state-space matrices
$[A_a]$	=	aerodynamic stiffness matrix
a, b	=	panel length and width
$[\bar{C}]$	=	modal damping matrix
$\{d\}$	=	piezoelectric coupling constants
$\{E_i\}$	=	electrical field, $i = 1, 2, 3$
$[G]$	=	aerodynamic damping matrix
h	=	thickness
$[K]$	=	linear stiffness matrix
$\boldsymbol{K}$, $\boldsymbol{K}_e$	=	state feedback and estimator gain matrices
$[K_q]$, $[K_{qq}]$	=	modal quadratic and cubic stiffness matrices
$[K1]$, $[K2]$	=	first- and second-order nonlinear stiffness matrix
$[\bar{K}]$	=	modal stiffness matrix
$[M]$	=	mass matrix
$\{M\}$, $\{N\}$, $\{R\}$	=	bending moment, in-plane, and shear stress resultants
$[\bar{M}]$	=	modal mass matrix
$\boldsymbol{Q}$, $\boldsymbol{R}$	=	controller weighting matrices
$\boldsymbol{Q}_e$, $\boldsymbol{R}_e$	=	estimator weighting matrices
$[\bar{Q}]$	=	transformed reduced lamina stiffness matrix
$\{q\}$	=	modal coordinate vector
q_a	=	dynamic pressure
$\{q^s\}$	=	sensor charge output vector
$\boldsymbol{U}$	=	control input vector
u, v, w	=	displacements
V	=	electrical voltage
$\{W\}$	=	system nodal degree of freedom (DOF)
$\boldsymbol{X}$, $\hat{\boldsymbol{X}}$	=	actual and estimated state vectors
$\boldsymbol{Y}$	=	output vector
α	=	flow yaw angle
γ	=	shear strain
$\boldsymbol{\Delta} A_q$	=	nonlinear state matrix
Δp_a	=	aerodynamic pressure
ε	=	strain
$\{\kappa\}$	=	curvature vector
λ	=	nondimensional dynamic pressure
ρ	=	mass density
σ, τ	=	stress components
$[\boldsymbol{\Phi}]$	=	modal matrix
ψ_x, ψ_y	=	rotations of the normal about x and y axes

Received 8 August 2002; accepted for publication 1 October 2004.

*Engineer/Scientist.
†Ph.D. Student, Department of Aerospace Engineering. Student Member AIAA.
‡Senior Systems Engineer, Department of Architecture.
§Professor, Department of Aerospace Engineering. Associate Fellow AIAA.

Subscripts

a	=	air
b	=	transverse bending DOF
L	=	linear
m	=	membrane DOF
N	=	membrane force
NL	=	nonlinear
θ	=	large deflection
ϕ	=	electrical

I. Introduction

RECENTLY, there has been a renewed interest in flight vehicles that operate at high supersonic and hypersonic Mach numbers, such as the X-33 advanced technology demonstrator, the X-34 reusable technology demonstrator for a launch vehicle, and the recent NASA Space Launch Initiative (SLI) Project to develop second-generation reusable launch vehicles. The exterior panels of such vehicles will be affected by supersonic panel flutter phenomena. Supersonic panel flutter is a self-excited oscillation of panels exposed to aerodynamic flow with high Mach numbers. As the flow dynamic pressure increases, the panel stiffness is modified by the aerodynamic loading such that the first mode natural frequency increases, whereas the second mode natural frequency decreases. At the flutter boundary, the two modes coalesce, and the panel motion becomes unstable based on linear structure theory. However, due to the structural nonlinearities (in-plane stretching forces) the panel motion is limited to a constant amplitude limit-cycle oscillation (LCO). The amplitude of the LCO grows as the dynamic pressure increases.

Since the late 1950s and early 1960s, there have been many papers in the literature addressing nonlinear panel flutter. An excellent review paper with an extensive review of various analytical and experimental results for nonlinear supersonic and hypersonic panel flutter up to 1999 is given by Mei et al.[1] Friedmann and Hanin[2] were the first to study the supersonic nonlinear flutter of rectangular isotropic and orthotropic panels with arbitrary flow direction using the first-order piston theory for aerodynamic pressure and Galerkin's method in the spatial domain. Abdel-Motagaly et al.[3] have recently used the finite element method to study the nonlinear flutter of composite panels with yawed supersonic flows by extending the three-mode triangular Mindlin (MIN3) triangular element developed by Tessler and Hughes.[4] It was found that, for laminated composite panels, the flow direction could greatly affect the limit-cycle behavior and panel deflection shape.

The requirements of energy-efficient, high-strength, and minimum-weight vehicles have generated an interest in the use of smart or adaptive materials such as piezoelectric ceramics that are attached or embedded into the panels to control and suppress undesired panel vibrations. Scott and Weisshaar[5] were the first to study the suppression of linear panel flutter using piezoelectric materials for simply supported isotropic panels modeled with the Ritz method and linear quadratic regulator (LQR) full-state feedback. It was concluded that bending moment actuation is not effective in controlling linear panel flutter. This is because linear flutter models neglect structural nonlinearities and, hence, overestimate the panel response beyond the linear flutter boundary. Surace et al.[6] used piezoelectric sensors and actuators to suppress the linear supersonic flutter of composite panels using Galerkin's method and structured singular value robust control techniques. Frampton et al.[7] employed a collocated direct rate feedback control scheme for the active control of linear panel flutter. The linearized potential flow aerodynamics were used for the full transonic and supersonic Mach number range. Lai et al.[8] studied the control of nonlinear flutter of a simply supported isotropic plate using piezoelectric actuators. The plate was modeled with Galerkin's method to obtain the nonlinear modal equations, and the LQR control method was employed based on the linearized modal equations. It was concluded that the bending moment induced by piezoelectric actuators is much more effective than induced in-plane forces for nonlinear panel flutter suppression. Zhou et al.[9,10] used the finite element method and LQR full-state feedback to control isotropic and composite panels with surface bonded or embedded piezoelectric patches. The norms of the feedback control gain (NFCG) were used to provide the optimal shape and location of the piezoelectric actuators. Numerical simulations showed that the critical flutter dynamic pressure can be increased up to four times and upto two times for simply supported and clamped isotropic panels, respectively. Dongi et al.[11] have presented a finite element method for adaptive panels with self-sensing piezoelectric actuators. A control approach based on output feedback for active compensation of aerodynamic stiffness terms was developed and shown to be able to increase the flutter boundary Mach number from 3.22 to 6.67 for a simply supported isotropic panel. Wind-tunnel testing performed by Ho et al.[12] has shown that panel limit-cycle motions observed in the wind tunnel can be successfully reduced for composite panels with one-sided surface-mounted piezoelectric actuators and strain sensors by the use of an iterative root locus based gain tuning algorithm. The wind-tunnel testing showed the leading-edge piezoelectric actuator patches to be more effective than the trailing-edge patches in suppressing panel flutter. Kim and Moon[13] presented a comparison between active control and passive damping using piezoelectric actuators for nonlinear panel flutter. The finite element method was used to model the panel and the LQR control method was applied for active flutter control. The shape and location of the piezoelectric actuators was determined by the use of genetic algorithms. With this exhaustive search for panel flutter suppression studies, two main findings are determined. First, the effect of flow yaw angle has never been considered in the literature for both linear and nonlinear panel flutter suppression, despite its great practical importance and its effect on the panel flutter mode shape and, consequently, on the optimal location of piezoelectric actuators and sensors. Second, most of the studies used LQR full-state feedback control under the assumption that all of the states are available without any consideration for the problem of state estimation for the nonlinear system dynamics.

In this paper, a coupled structural–electrical modal finite element formulation for composite panels, with embedded piezoelectric sensors and actuators, is presented and used to study nonlinear supersonic panel flutter suppression given the effect of airflow yaw angle. The first-order shear deformation theory is used for laminated composite panels and the von Kármán nonlinear strain–displacement relations are employed for large deflection response. structural–electrical coupling is considered by the use of the linear piezoelectricity constitutive relations. The coupled nonlinear equations of motion are derived by extending the MIN3 plate element with improved transverse shear.[4] Additional electrical degrees of freedom (DOF) per each piezoelectric layer are used to handle piezoelectric sensors and actuators. The system equations of motion in the structure node DOF are transformed into the modal coordinates with the panel linear vibration modes to obtain a reduced set of nonlinear dynamic modal equations that are suitable for controller design. The presented finite element modal formulation is validated by comparison with other finite element and analytical solutions. A comparison is presented between the effectiveness of the linear quadratic Gaussian (LQG) controller and the nonlinear output controller, comprising an LQR and an extended Kalman filter (EKF) nonlinear state estimator (LQR/EKF), in suppressing nonlinear panel flutter. The optimal location of piezoelectric layers is determined based on closed-loop criteria by the use of the NFCG for actuators and the norm of Kalman filter estimator gains (NKFEG) for sensors. Numerical simulations are presented for isotropic and composite panels to show the effectiveness of the proposed active control methodology in controlling nonlinear panel flutter at different flow yaw angles.

II. Finite Element Formulation

A. Equations of Motion in Structure Node DOF

The MIN3 plate element with improved transverse shear, developed by Tessler and Hughes,[4] is extended and used in this study. The MIN3 element is modified by the addition of an additional DOF per piezoelectric layer to model piezoelectric sensors and actuators.

The modified MIN3 element nodal DOF are defined as

$$\{w\}^T = \lfloor \lfloor w_b \rfloor \quad \lfloor w_m \rfloor \quad \lfloor w_\phi \rfloor \rfloor \tag{1}$$

$$\{w_b\}^T = \lfloor w_1 \quad w_2 \quad w_3 \quad \psi_{x1} \quad \psi_{x2} \quad \psi_{x3} \quad \psi_{y1} \quad \psi_{y2} \quad \psi_{y3} \rfloor$$

$$\{w_m\}^T = \lfloor u_1 \quad u_2 \quad u_3 \quad v_1 \quad v_2 \quad v_3 \rfloor$$

$$\{w_\phi\}^T = \lfloor V_1 \quad \cdots \quad V_{\text{np}} \rfloor \tag{2}$$

where np is the total number of piezoelectric layers per element. The electrical potential DOF is assumed constant for each piezoelectric layer, that is, w_ϕ is assumed constant over the element area. The von Kármán large deflection strain–displacement relations for a plate undergoing extension and bending at any point z through the plate thickness and with use of Mindlin first-order shear deformation theory are given by

$$\{e\} = \{e^0\} + z\{\kappa\} = \left\{e_m^0\right\} + \left\{e_\theta^0\right\} + z\{\kappa\} = \left\{e_m^0\right\} + \tfrac{1}{2}[\theta]\{\theta\} + z\{\kappa\}$$

$$\{\gamma\} = \begin{Bmatrix} \gamma_{yz} \\ \gamma_{xz} \end{Bmatrix} = \begin{Bmatrix} w_{,y} \\ w_{,x} \end{Bmatrix} + \begin{Bmatrix} \psi_x \\ \psi_y \end{Bmatrix} \tag{3}$$

where

$$\{\varepsilon\} = \begin{Bmatrix} \varepsilon_x \\ \varepsilon_y \\ \gamma_{xy} \end{Bmatrix}, \qquad \left\{e_m^0\right\} = \begin{Bmatrix} u_{,x} \\ v_{,y} \\ u_{,y} + v_{,x} \end{Bmatrix}$$

$$\{\kappa\} = \begin{Bmatrix} \psi_{y,x} \\ \psi_{x,y} \\ \psi_{x,x} + \psi_{y,y} \end{Bmatrix}, \qquad [\theta] = \begin{bmatrix} w_{,x} & 0 \\ 0 & w_{,y} \\ w_{,y} & w_{,x} \end{bmatrix}$$

$$\{\theta\} = \begin{Bmatrix} w_{,x} \\ w_{,y} \end{Bmatrix} \tag{4}$$

where a comma denotes derivative with respect to the subscript. The piezoelectric layers electrical field–potential relations are analogous to mechanical strain–displacement relations. If constant electrical DOF is assumed over each piezoelectric layer in the element, the relationship between electrical field and electrical DOF can be written as

$$\begin{Bmatrix} E_1 \\ \vdots \\ E_{\text{np}} \end{Bmatrix} = -[B_\phi]\{w_\phi\} = -\begin{bmatrix} \frac{1}{h_1} & \cdots & 0 \\ \vdots & \ddots & \vdots \\ 0 & \cdots & \frac{1}{h_{\text{np}}} \end{bmatrix} \begin{Bmatrix} V_1 \\ \vdots \\ V_{\text{np}} \end{Bmatrix} \tag{5}$$

For isotropic piezoelectric materials, the polarization direction is the "3" direction; consequently, $\{E_i\}$ is the electrical field in the 3 direction, and h_i is the thickness of the ith piezoelectric layer. The constitutive equations (stress–strain relationships) of the kth layer for a fiber reinforced laminated composite panel with embedded piezoelectric layers expressed in terms of stress resultants are

$$\begin{Bmatrix} N \\ M \end{Bmatrix} = \begin{bmatrix} A & B \\ B & D \end{bmatrix} \begin{Bmatrix} \varepsilon^0 \\ \kappa \end{Bmatrix} - \begin{Bmatrix} N_\phi \\ M_\phi \end{Bmatrix}, \qquad \{R\} = [A_s]\{\gamma\} \tag{6}$$

where the piezoelectric resultant force and moment are given by

$$(\{N_\phi\}, \{M_\phi\}) = \int_{-h/2}^{h/2} [\bar{Q}]_k \{d\}_k E_{ik}(1, z)\, \mathrm{d}z \tag{7}$$

In this study, bending moment piezoelectric actuation and sensing is assumed. In other words, the piezoelectric resultant in-plane force $\{N_\phi\}$ is zero. This is achieved by the use of a pair of self-sensing piezoelectric actuators (single piezoelectric layer used as actuator and sensor simultaneously[14]) at the top and bottom surfaces of the laminate and by the application of equal and opposite voltage to the two actuators. Thus, the element vector of electrical DOF $\{w_\phi\}$ becomes a scalar for each element because the electrical DOF at the pair of top and bottom piezoelectric layers are equal and opposite. This can be justified because it was concluded in previous work,[8,9] that bending moment actuation is much more efficient than in-plane tension for nonlinear panel flutter suppression. The supersonic aerodynamic pressure loading is expressed by the use of the first-order piston theory. This theory relates the aerodynamic pressure and panel transverse deflection as follows:

$$\Delta p_a = -(2q_a/\beta)\Big\{w_{,x}\cos\alpha + w_{,y}\sin\alpha + \Big[\Big(M_\infty^2 - 2\Big)\Big/\Big(M_\infty^2 - 1\Big)\Big](1/V_\infty)w_{,t}\Big\} \tag{8}$$

where $q_a = \rho_a V_\infty^2/2$ is the dynamic pressure, ρ_a is the air density, V_∞ is the airflow velocity, w is the panel transverse displacement, M_∞ is the Mach number, α is the flow yaw angle with the panel x axis, and $\beta = \sqrt{(M_\infty^2 - 1)}$. By the use of nondimensional parameters, Eq. (8) can be written as

$$\Delta p_a = -\Big[\lambda\Big(D_{110}\Big/a^3\Big)(w_{,x}\cos\alpha + w_{,y}\sin\alpha) + (g_a/\omega_0)\Big(D_{110}\Big/a^4\Big)w_{,t}\Big] \tag{9}$$

where

$$\lambda = \frac{2q_a a^3}{\beta D_{110}}, \qquad g_a = \frac{\rho_a V_\infty \Big(M_\infty^2 - 2\Big)}{\rho h \omega_o \beta^3}$$

$$c_a = \frac{g_a^2}{\lambda}, \qquad \omega_o = \sqrt{\frac{D_{110}}{\rho h a^4}} \tag{10}$$

are the nondimensional dynamic pressure, nondimensional aerodynamic damping, aerodynamic damping coefficient, and panel reference frequency, respectively. D_{110} is the first entry of the laminate bending stiffness matrix $[D]$ determined with all fibers of the composite layers in the x direction as a reference.

By the use of Hamilton's principle, finite element expressions, and standard finite element assembly procedure, the nonlinear equations of motion in structure node DOF for composite panels with embedded self-sensing piezoelectric actuators under yawed supersonic flow can be written as follows.

Actuator equation:

$$\frac{1}{\omega_0^2}\begin{bmatrix} M_b & 0 \\ 0 & M_m \end{bmatrix}\begin{Bmatrix} \ddot{W}_b \\ \ddot{W}_m \end{Bmatrix} + \frac{g_a}{\omega_0}\begin{bmatrix} G_a & 0 \\ 0 & 0 \end{bmatrix}\begin{Bmatrix} \dot{W}_b \\ \dot{W}_m \end{Bmatrix} + \left(\lambda\begin{bmatrix} A_a & 0 \\ 0 & 0 \end{bmatrix} + \begin{bmatrix} K_b & K_{bm} \\ K_{mb} & K_m \end{bmatrix} + \begin{bmatrix} K1_b + K1_{Nm} + K1_{Nb} & K1_{bm} \\ K1_{mb} & 0 \end{bmatrix} + \begin{bmatrix} K2 & 0 \\ 0 & 0 \end{bmatrix}\right)\begin{Bmatrix} W_b \\ W_m \end{Bmatrix} = -\begin{bmatrix} K_{b\phi} \\ 0 \end{bmatrix}\{W_\phi\} \tag{11}$$

Sensor equation:

$$\{q^s\} = -[K_{\phi b} \quad 0]\begin{Bmatrix} W_b \\ W_m \end{Bmatrix} \tag{12}$$

where $\{W\} = \{W_b, W_m\}^T$ is the panel unknown displacement. The nonlinear stiffness matrices $[K1]$ and $[K2]$ depend linearly and quadratically on the unknown displacements, respectively. The detailed derivation of Eqs. (11) and (12) can be found in Ref. 15. When the in-plane mass matrix $[M_m]$ is neglected, the in-plane DOF $\{W_m\}$ can be expressed in terms of the bending DOF $\{W_b\}$ as follows:

$$\{W_m\} = -[K_m]^{-1}([K_{mb}] + [K1_{mb}])\{W_b\} \tag{13}$$

and the system equations can be expressed in terms of the bending displacement $\{W_b\}$ only as

$$\Big(1\Big/\omega_0^2\Big)[M_b]\{\ddot{W}_b\} + (g_a/\omega_0)[G_a]\{\dot{W}_b\} + ([K_L] + [K_{\text{NL}}])\{W_b\} = -[K_{b\phi}]\{W_\phi\} \tag{14}$$

where the linear and nonlinear stiffness matrices are given by

$$[K_L] = \left(\lambda[A_a] + [K_b] - [K_{bm}][K_m]^{-1}[K_{mb}]\right) \tag{15}$$

$$[K_{\mathrm{NL}}] = -[K_{bm}][K_m]^{-1}[K1_{mb}] + [K1_b] + [K1_{Nm}] + [K1_{Nb}] + [K2] - [K1_{bm}][K_m]^{-1}([K_{mb}] + [K1_{mb}]) \tag{16}$$

The system equation of motion in structural DOF, Eq. (14), has two major drawbacks. First, the element nonlinear stiffness matrices have to be evaluated and the system nonlinear stiffness $[K_{\mathrm{NL}}]$ has to be assembled and updated at each numerical integration step. Second, the number of structure node DOF $\{W_b\}$ is usually very large. To overcome these drawbacks, the system equations are reduced with modal transformation and modal reduction based on the values of modal participation. This results in a system of coupled nonlinear modal equations with a smaller number of DOF, which in turn could be used for control design and numerical integration.

B. Equations of Motion in Modal Coordinates

If the panel deflection can be expressed as a linear combination of some known function as

$$\{W_b\} = \sum_{r=1}^{n} q_r(t)\{\phi_r\} = [\Phi]\{q\} \tag{17}$$

where the number of retained linear modes n is much smaller than the number of structure node DOF in bending $\{W_b\}$, then the normal mode $\{\phi_r\}$, which is normalized with the maximum component to unity, and the linear natural frequency ω_r are obtained from the linear vibration of the system. By the use of Eq. (17) as a substitute for the unknown bending DOF $\{W_b\}$, the reduced nonlinear panel flutter equations in modal coordinates can be expressed as follows.

Actuator modal equation:

$$\left(1/\omega_0^2\right)[\bar{M}_b]\{\ddot{q}\} + (g_a/\omega_0)[\bar{G}]\{\dot{q}\} + 2\zeta_r\omega_r\left(M_r/\omega_0^2\right)[I]\{\dot{q}\} + ([\bar{K}_L] + [K_q] + [K_{qq}])\{q\} = -[\bar{K}_{b\phi}]\{W_\phi\} \tag{18}$$

Sensor modal equation:

$$\{q^s\} = -[\bar{K}_{\phi b}]\{q\} \tag{19}$$

The detailed expressions for the modal matrices can be found in Refs. 15 and 16. A structural damping modal matrix, $[\bar{C}] = 2\zeta_r\omega_r(M_r/\omega_0^2)[I]$, has been added to Eq. (18), where ζ_r, ω_r, and M_r are the modal damping, frequency, and mass, respectively, and $[I]$ is the identity matrix. The modal damping ratio can be determined based on testing or on the performance of similar structures. The number of modes required can be determined by the use of the modal participation value, which is defined as

$$\text{participation of the } r\text{th mode} = |q_r| \Big/ \sum_{i=1}^{n} |q_i| \tag{20}$$

For the problem of nonlinear panel flutter, the number of modes needed for a converged LCO can be determined based on the modal participation values.[3,16] This guarantees an accurate flutter deflection shape, which is crucial for panel flutter suppression. The advantages of the modal equations of motion given by Eq. (18) are as follows: 1) There is no need to assemble and update the modal nonlinear stiffness matrices $[K_q]$ and $[K_{qq}]$ at each time step because they are explicit functions of the unknown modal coordinates $\{q\}$. 2) The number of modal equations is much smaller than the number of structural equations. This modal approach has been demonstrated for nonlinear panel flutter of composite panels by the use of time-domain numerical integration by Zhou et al.[9] and by the use of the linearized updated model with nonlinear time function (LUM/NTF) frequency-domain solution method by Abdel-Motagaly et al.[3] It was also applied to nonlinear panel response under combined aerodynamic and acoustic loading by Abdel-Motagaly et al.[16]

III. Control Methodology

A. Controller Design

The nonlinear modal equations of motion given by Eqs. (18) and (19) can be expressed in the standard state-space form as follows

$$\dot{\boldsymbol{X}} = (\boldsymbol{A} + \boldsymbol{\Delta A}_q)\boldsymbol{X} + \boldsymbol{BU}, \qquad \boldsymbol{Y} = \boldsymbol{CX} + \boldsymbol{DU} \tag{21}$$

where

$$\boldsymbol{X} = \begin{Bmatrix} q \\ \dot{q} \end{Bmatrix}, \qquad \boldsymbol{U} = \{W_\phi\}, \qquad \boldsymbol{Y} = \{q^s\} \tag{22}$$

$$[\boldsymbol{A}] = \begin{bmatrix} [0] & [I] \\ -\omega_0^2[\bar{M}_b]^{-1}[\bar{K}_L] & -\omega_0^2[\bar{M}_b]^{-1}[\bar{C}_d] \end{bmatrix}$$

$$[\boldsymbol{\Delta A}_q] = \begin{bmatrix} [0] & [0] \\ -\omega_0^2[\bar{M}_b]^{-1}([K_q] + [K_{qq}]) & [0] \end{bmatrix}$$

$$[\boldsymbol{B}] = \begin{bmatrix} [0] \\ -\omega_0^2[\bar{M}_b]^{-1}[\bar{K}_{b\phi}] \end{bmatrix}, \qquad [\boldsymbol{C}] = [[\bar{K}_{\phi b}] \quad [0]]$$

$$[\boldsymbol{D}] = [0] \tag{23}$$

The modal damping matrix $[\bar{C}_d]$ contains both modal aerodynamic and modal structural damping terms. The system matrix $[\boldsymbol{\Delta A}_q]$ represents the effect of nonlinear stiffness of the panel. By the use of linearization about the system reference point (point with no deflection, $\{q\} = 0$), the nonlinear system matrix vanishes at this reference point (because they are homogeneous functions of $\boldsymbol{X}$), and the state-space model in Eq. (21) reduces to the standard linear state-space equations.

1. LQG Controller

The LQG controller is based on the linear systems separation principle that allows separate design of a feedback control gain and of an observer gain to form a dynamic compensator. The LQR full-state feedback and the linear Kalman filter estimator are combined together to form the LQG controller. The controller output is given by

$$\boldsymbol{U} = -\boldsymbol{K}\hat{\boldsymbol{X}} \tag{24}$$

where the LQR gain $\boldsymbol{K}$ seeks a solution for the linear full-state feedback problem that minimizes a quadratic performance index,

$$\boldsymbol{J} = \int_0^\infty [\boldsymbol{X}^T \quad \boldsymbol{QX} + \boldsymbol{U}^T \quad \boldsymbol{RU}]\,\mathrm{d}t \tag{25}$$

where $\boldsymbol{Q}$ is a symmetric positive semidefinite state weighting matrix and $\boldsymbol{R}$ is a symmetric positive definite control effort weighting matrix. The solution for the controller gains that minimize the performance index is given by

$$\boldsymbol{K} = \boldsymbol{R}^{-1}\boldsymbol{B}^T\boldsymbol{P} \tag{26}$$

where $\boldsymbol{P}$ is a positive definite symmetric matrix determined from the solution of the algebraic Riccati equation given in Ref. 17,

$$\boldsymbol{A}^T\boldsymbol{P} + \boldsymbol{PA} - \boldsymbol{PBR}^{-1}\boldsymbol{B}^T\boldsymbol{P} + \boldsymbol{Q} = \boldsymbol{0} \tag{27}$$

The estimated state vector is determined with the optimal linear estimator (Kalman filter) that minimizes the state estimation error. The standard fixed gain linear Kalman filter estimator can be described by the following dynamic equations[17]:

$$\dot{\hat{\boldsymbol{X}}} = \boldsymbol{A}\hat{\boldsymbol{X}} + \boldsymbol{BU} + \boldsymbol{K}_e(\boldsymbol{Y} - \boldsymbol{C}\hat{\boldsymbol{X}})$$

$$\boldsymbol{AP}_e + \boldsymbol{P}_e\boldsymbol{A}^T - \boldsymbol{P}_e\boldsymbol{C}^T\boldsymbol{R}_e^{-1}\boldsymbol{CP}_e + \boldsymbol{Q}_e = \boldsymbol{0}, \qquad \boldsymbol{K}_e = \boldsymbol{P}_e\boldsymbol{C}^T\boldsymbol{R}_e^{-1}$$

$$\boldsymbol{P}_e = \boldsymbol{E}\{\boldsymbol{ee}^T\}, \qquad \boldsymbol{e} = \boldsymbol{X} - \hat{\boldsymbol{X}} \tag{28}$$

where $\boldsymbol{P}_e$ is the error covariance matrix and $\boldsymbol{e}$ is the state estimation error. Some tuning is required to select $\boldsymbol{R}_e$ and $\boldsymbol{Q}_e$ to achieve good filter performance.

2. LQR/EKF Controller

One major drawback with the application of the LQG controller to the problem of nonlinear panel flutter suppression is that the nonlinear effects are not considered at all in the estimation process due to the use of a linear Kalman filter estimator. One solution to such a problem is to use the EKF state estimator in conjunction with LQR to form a nonlinear dynamic output compensator, referred to in this study as the LQR/EKF controller. In Ref. 18, the dynamic equations of an EKF are given by

$$\dot{\hat{\boldsymbol{X}}} = \bar{\boldsymbol{A}}\hat{\boldsymbol{X}} + \boldsymbol{B}\boldsymbol{U} + \boldsymbol{K}_e(\boldsymbol{Y} - \boldsymbol{C}\hat{\boldsymbol{X}})$$

$$\dot{\boldsymbol{P}}_e = \bar{\boldsymbol{A}}\boldsymbol{P}_e + \boldsymbol{P}_e\bar{\boldsymbol{A}}^T - \boldsymbol{P}_e\boldsymbol{C}^T\boldsymbol{R}_e^{-1}\boldsymbol{C}\boldsymbol{P}_e + \boldsymbol{Q}_e, \qquad \boldsymbol{K}_e = \boldsymbol{P}_e\boldsymbol{C}^T\boldsymbol{R}_e^{-1}$$

$$\bar{\boldsymbol{A}} = \boldsymbol{A} + \boldsymbol{\Delta A}_q(\hat{\boldsymbol{X}}) \tag{29}$$

where the term $\boldsymbol{\Delta A}_q(\hat{\boldsymbol{X}})$ represents the nonlinear state-space matrix evaluated with the current state estimate. Unlike the standard fixed gain Kalman filter, the EKF gain sequence cannot be predetermined and has to be evaluated online.

B. Placement of Piezoelectric Actuators and Sensors

The method adopted for actuator placement in this study is the method of matrix NFCG.[8–10] This method determines the effectiveness of a piezoelectric actuator by the use of the norm of feedback gain designed with LQR

$$\text{NFCG} = \|\boldsymbol{K}_{\text{LQR}}\|_2 \tag{30}$$

The higher the value of NFCG, the more effective the actuator is for panel flutter suppression. The NFCG method is extended for optimal sensor location by the use of the NKFEG that determines the effectiveness of a piezoelectric sensor with the norm of feedback gain designed by the use of the linear Kalman filter

$$\text{NKFEG} = \|\boldsymbol{K}_{\text{Kalman}}\|_2 \tag{31}$$

The higher the value of NKFEG, the more effective the sensor is for the problem of state estimation.

IV. Results and Discussion

A. Finite Element Validation

The accuracy of the present formulation is first validated by comparison with other finite element and analytical solutions. Material properties for the isotropic, composite, and piezoelectric materials used are given in Table 1. The first validation test involves evaluation of the LCO response of nonlinear panel flutter. The LCO response for a simply supported (with immovable inplane edges) square $12 \times 12 \times 0.05$ in. ($30.5 \times 30.5 \times 0.13$ cm) isotropic panel with zero yaw angle by the use of a 12×12 MIN3 mesh and six modes in the x direction are shown in Fig. 1a with both LUM/NTF frequency[3] and time-domain numerical integration methods. The LCO response obtained in Ref. 15 by the use of a six-mode model with Galerkin's method and numerical integration is also shown in Fig. 1 for comparison. The aerodynamic damping coefficient c_a is set to 0.1. [See Eq. (10)]. Both time- and frequency-domain solutions found with the present modal MIN3 element formulation are shown to be in good agreement with the analytical solution. For composite panels, the LCO results of a simply supported eight-layer $[0/45/-45/90]_S$ graphite/epoxy square $12 \times 12 \times 0.048$ in. ($30.5 \times 30.5 \times 0.12$ cm) panel obtained in Ref. 10 by the use of the C^1 conforming rectangular plate element and time-domain modal formulation are compared with those obtained with the present formulation. The complete plate is modeled with 12×12 mesh and six modes in the x direction. The LCO response at zero yaw angle, shown in Fig. 1b, demonstrates the accuracy of the MIN3 element and the present finite element formulation in predicting the nonlinear panel flutter response of

Table 1 Material properties

Property	Value
	Isotropic (aluminum)
E	10.5 Msi[a] (72.4 GPa)
ν	0.3
ρ	0.2588×10^{-3} lb $\cdot$ s^2/in.^{4} (2700 kg/m^3)
	Composite (graphite/epoxy)
E_1	22.5 Msi (155.1 GPa)
E_2	1.17 Msi (8.1 GPa)
G_{12}	0.66 Msi (4.6 GPa)
G_{23}	0.44 Msi (3.0 GPa)
ν_{12}	0.22
ρ	0.1458×10^{-3} lb $\cdot$ s^2/in.^{4} (1550 kg/m^3)
	PVDF
E	0.29 Msi (2.0 GPa)
ν_{12}	0.29
$d_{31} = d_{32}$	0.87×10^{-9} in./V (22×10^{-12} m/V)
	PZT5A
$E_1 = E_2$	9.9 Msi (68.3 GPa)
$G_{12} = G_{23}$	3.82 Msi (26.3 GPa)
$d_{31} = d_{32}$	-6.73×10^{-9} in./V (-171×10^{-12} m/V)
ρ	0.72×10^{-3} lb $\cdot$ s^2/in.^{4}(7700 kg/m^3)
ν_{12}	0.31
$E_{\max}$	15240 V/in. (600×10^3 V/m)

[a]Msi, mega square inch.

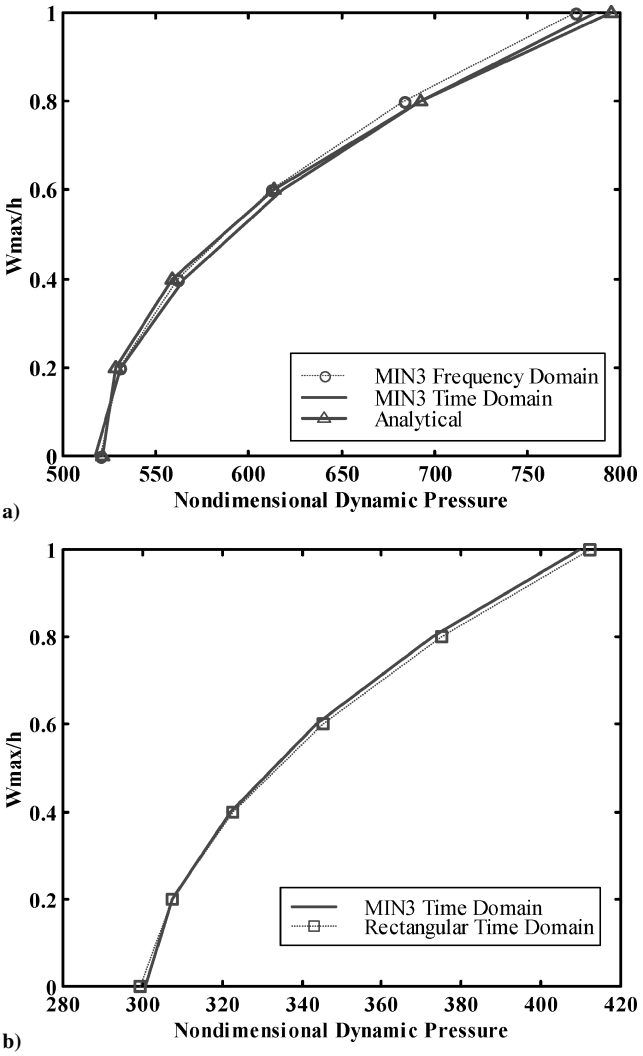

Fig. 1 Validation of flutter limit-cycle amplitude for simply supported panels: a) square isotropic and b) square [0/45/−45/90]$_S$ composite laminate.

Table 2 Comparison of static deflection for the piezoelectric bimorph beam (10^{-7} m) using finite element solutions

	X, cm				
Method	2.0	4.0	6.0	8.0	10.0
Solid FE[19]	0.138	0.552	1.242	2.208	3.450
QUAD4[20]	0.14	0.55	1.24	2.21	3.45
MIN3	0.149	0.587	1.289	2.256	3.487

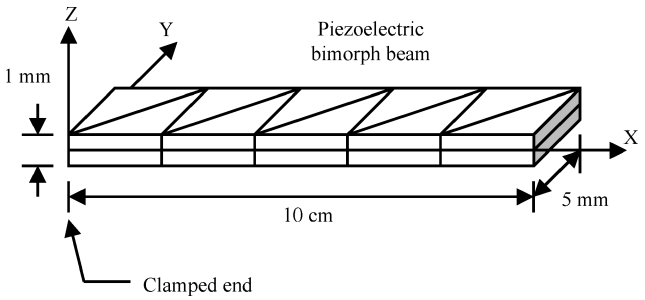

Fig. 2 Clamped PVDF piezoelectric bimorph beam modeled with MIN3 elements.

composite panels. The piezoelectric finite element formulation is validated using the cantilevered bimorph beam shown in Fig. 2. The bimorph beam consists of two identical polyvinylidene fluoride (PVDF) piezoelectric layers with polling axis in the 3 direction but with opposite polarities. A unit of electrical voltage is applied across the thickness, and the beam lateral deflection at different points is determined. The results obtained using a 5×2 MIN3 element mesh are compared vs the solid finite element of Ref. 19 and the QUAD4 finite element of Ref. 20. Table 2 shows that the present MIN3 element formulation is in good agreement with other finite element solutions.

B. Effect of Flow Yaw Angle on Nonlinear Panel Flutter

The effect of flow yaw angle α on nonlinear panel flutter LCO is presented in this section. The frequency domain LUM/NTF method is used in this section because it is more efficient computationally than the time-domain numerical integration method for analysis purposes. Because LCO is a periodic motion, by the use of the LUM/NTF method, the modal equations are assumed to have a periodic solution, and the corresponding eigenvalue problem is iteratively solved for the updated equivalent linear system until convergence of the eigenvector is reached.[3]

The aerodynamic damping coefficient c_a is set to 0.01 for all cases, and the structural damping is neglected. Two simply supported panels are considered: a square $30.5 \times 30.5 \times 0.13$ cm isotropic panel and a rectangular $30.5 \times 30.5 \times 0.12$ cm graphite/epoxy eight-layer $[0/45/-45/90]_S$ composite panel. Both panels are modeled using a 12×12 mesh or 288 MIN3 elements. The number of structural DOF $\{W_b\}$ is 407, and it is reduced to the modal coordinates to include n selected modes.

First, modal convergence is studied for the isotropic panel to show the effect of yaw angle on the number of required modes. Modal convergence is confirmed by the convergence of the nondimensional dynamic pressure λ vs the number of modes used as shown in Fig. 3. Figure 3 shows that a 16-mode model is required for all yaw angles to yield a convergent LCO amplitude compared to the well-known six-mode model[21] in the x direction for a 0-deg yaw angle. Similar analysis for the rectangular composite panel shows that 16 modes are also required to obtain convergent LCO response.

Figure 4 shows the effect of flow yaw angle on LCO amplitude for square isotropic and rectangular composite panels. The variation of LCO amplitude vs nondimensional dynamic pressure for the isotropic panel at $\alpha = 0$, 15, 30, and 45 deg is given in Fig. 4a. Note that an increase in the flow angle has the effect of slightly increasing the critical nondimensional dynamic pressure λ_{cr} at zero LCO amplitude. However, as the LCO amplitude W_{max}/h increases, the difference in λ between different flow angles decreases. This effect

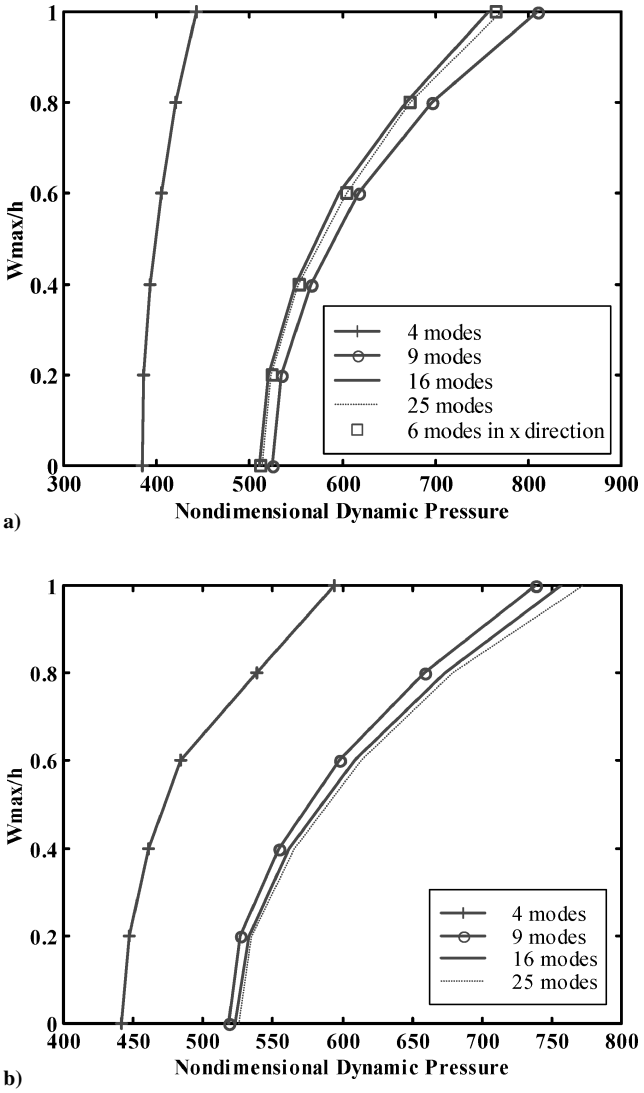

Fig. 3 Modal convergence for simply supported isotropic panel at α = a) 0 and b) 45 deg.

is due to the different nonlinear effect resulting from having different flutter mode shapes as the flow yaw angle changes. Figure 4b shows similar behavior for the rectangular composite panel but with larger separation than the square isotropic panel case. The flutter deflection shapes for the square isotropic panel at $W_{max}/h = 1.0$ and different yaw angles are given in Fig. 5. Note how the flow yaw angle greatly changes the flutter deflection shape. This necessitates having different actuator and sensor locations for different yaw angles, as will be seen in the next section.

C. Nonlinear Panel Flutter Suppression

1. Square Isotropic Panel

A square simply supported isotropic panel $30.5 \times 30.5 \times 0.13$ cm is used to study panel flutter suppression under a range of flow yaw angles. Self-sensing piezoelectric layers (PZT5A) are embedded on the top and bottom surfaces of the panel to avoid disturbing the airflow. The piezoelectric thickness is selected as 0.01 in. (0.025 cm) compared to the panel total thickness of 0.05 in. (0.13 cm). With use of this thickness, the actuation voltage is then limited to 152 V. (See Table 1 for the properties of PZT5A.) The aerodynamic damping coefficient c_a is assumed 0.01, and a structural modal damping ratio of 1% is added for all modes. The panel is modeled with a 10×10 finite element mesh, and the nonlinear modal equations of motion are derived using the 16-mode model, from mode (1,1) to (4,4). This results in a 32nd-order state-space system.

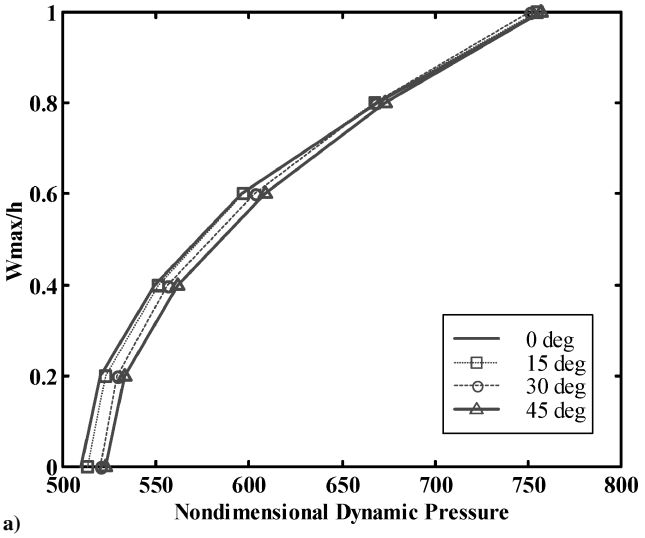

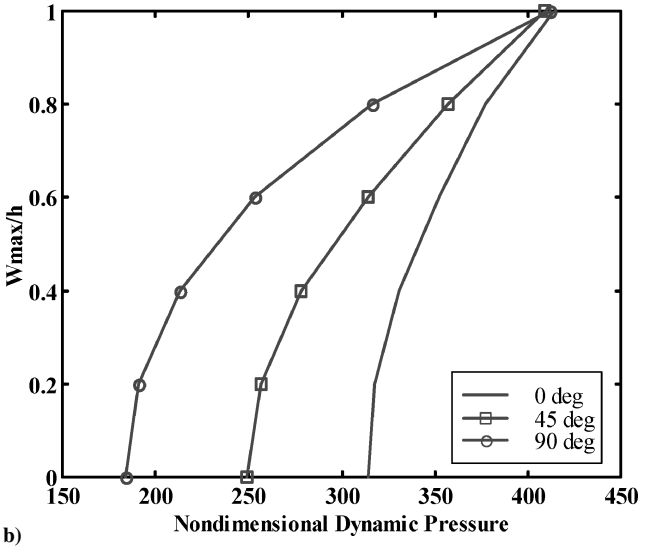

Fig. 4 Effect of flow yaw angle on limit-cycle amplitude for simply supported panels: a) square isotropic and b) rectangular [0/45/−45/90]*s* composite laminate.

The first step is determining the optimal location of the embedded piezoelectric layers to achieve optimal actuation and sensing. The panel is divided using a 10×10 mesh size and is completely covered on top and bottom with piezoelectric layers (total of 100 piezoelectric actuators/sensors). The linearized state-space equations are used to design both optimal feedback control (LQR) and optimal observer (Kalman filter). The state-weighting matrix $\boldsymbol{Q}$ is selected using the energy method, and the control-weighting matrix $\boldsymbol{R}$ is selected as a constant multiplied by the identity matrix

$$\boldsymbol{Q} = \begin{bmatrix} K & 0 \\ 0 & M \end{bmatrix}, \qquad \boldsymbol{R} = r[I] \tag{32}$$

and design parameters of the Kalman filters are selected as

$$\boldsymbol{Q}_e = [I], \qquad \boldsymbol{R}_e = [\boldsymbol{C}][\boldsymbol{C}]^T \tag{33}$$

The resulting optimal feedback gain $\boldsymbol{K}$ and observer gain $\boldsymbol{K}_e$ are matrices with sizes 100×32 and 32×100, respectively. They represent the feedback and the estimator gain vectors for each patch of the 100 piezoelectric patches used. The methods of NFCG and NKFEG are then used to determine the effectiveness of each piezoelectric patch for optimal actuation and sensing. Figure 6 shows the effect of flow angle on the optimal location of self-sensing piezoelectric actuators for different flow yaw angles within the range of 0–90 deg.

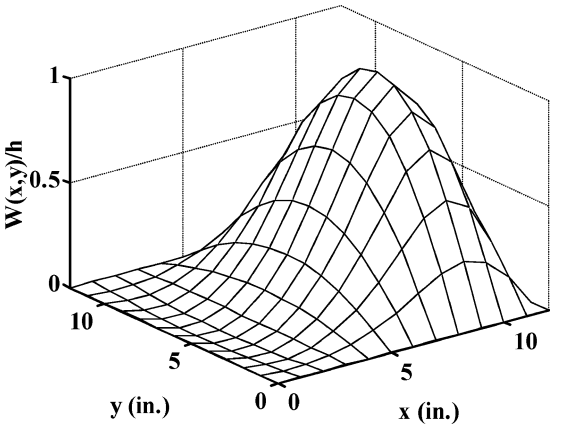

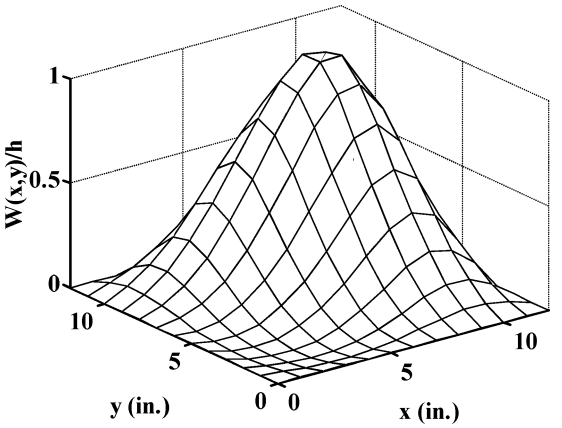

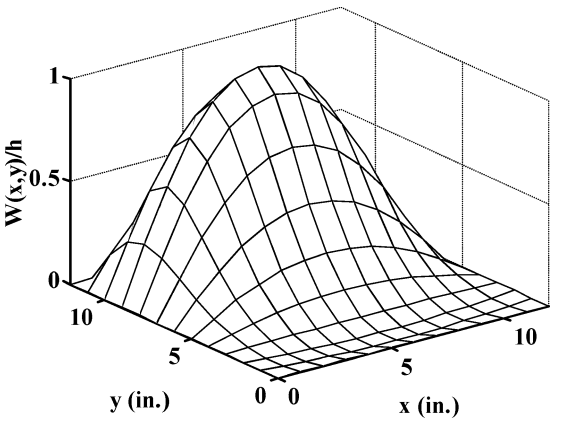

Fig. 5 Flutter deflection shape for simply supported isotropic square panel at different flow yaw angles.

The flow leading-edge (LE) piezoelectric patch is the optimal actuator location determined using NFCG, whereas the trailing-edge (TE) patch is the optimal sensor location determined using NKFEG. Rectangular-shaped piezoelectric patches are used to obtain practical sensor and actuator shapes. However, the optimal sensor and actuator shape can be refined by using more elements or triangular patches. Optimal sizing of piezoelectric actuators is outside the scope of this study, and, hence, the size of both sensor and actuator pieces is assumed by using the most effective 12 elements. This assumption is based on the studies described in Ref. 9 that showed that the optimal size of actuator is between 10 and 20% of the panel area for nonlinear panel flutter suppression. Because self-sensing piezoelectric actuators are utilized in this study, the size of both patches located at the LE (optimal actuator) and at the TE (optimal sensor) are assumed to be the same because both of them will be used

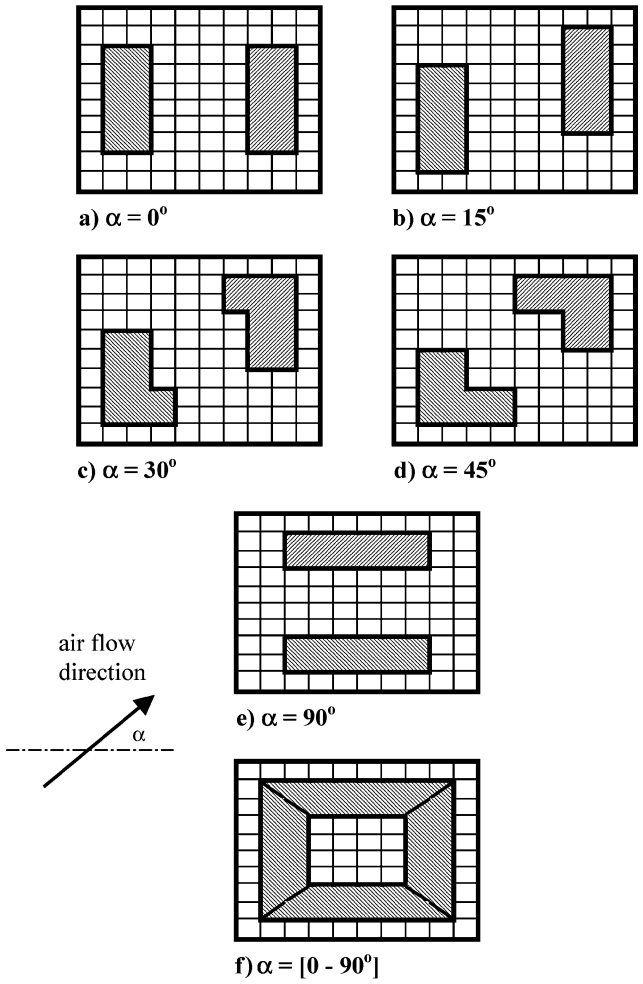

Fig. 6 Optimal actuator and sensor placement for square isotropic panel at different flow yaw angles ranging from 0 to 90 deg.

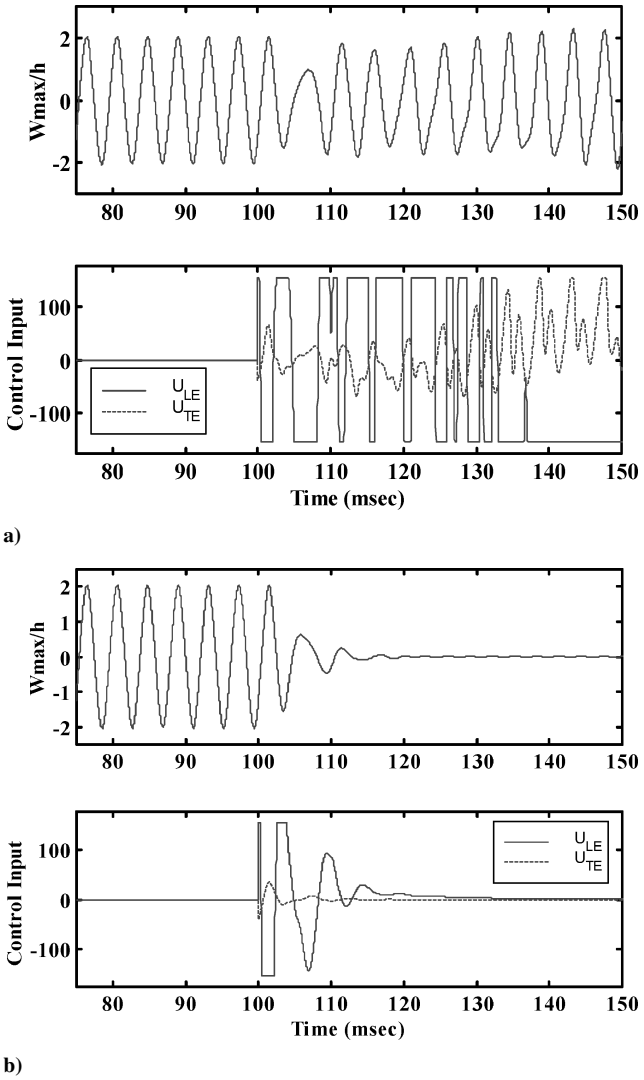

Fig. 7 Comparison between the performance of a) LQG controller and b) LQR/EKF nonlinear output controller for simply supported isotropic square panel at $\lambda = 1500$ and $\alpha = 0$ deg.

as actuators. In practice, other types of sensors may be used, such as accelerometers, displacement sensors, or strain gauges. Figure 6 clearly indicates how the change of flow angle has a major effect of the optimal actuator and sensor locations. In practice, it is required to design an active control system that includes piezoelectric placement for the panel, with the understanding that the panel will be subjected to a specific range of flow yaw angles. The range assumed in this study is from 0 to 90 deg. Performing optimization for piezoelectric placement over a range of α is not a simple task. A simpler methodology used in this study is to optimize the piezoelectric sensor and actuator placement for different angles within the specified range, as shown in Figs. 6a–6e, and then to group the resulting optimal locations together to find a single piezoelectric configuration that works over the entire range of angles. Figure 6f shows optimal actuator and sensor location that covers all of the yaw angles from 0 to 90 deg. The configuration in Figure 6f results in an outer square covering 48% of the panel surface with embedded PZT5A. The embedded piezoelectric is divided into four equal self-sensing actuators referred to as 0LE and 90LE for the leading-edge patches perpendicular to the 0- and 90-deg flow directions and 0TE and 90TE for the trailing-edge patches perpendicular to the 0- and 90-deg flow directions. On further examination of this configuration, it is seen that it does not only cover yaw angles from 0 to 90 deg, but, due to the panel symmetry and the usage of self-sensing actuators, this configuration will cover all angles from 0 to 360 deg.

The performance of LQG and LQR/EKF controllers is investigated based on their ability to suppress the panel nonlinear flutter. The measure used to assess flutter suppression performance is the maximum flutter-free dynamic pressure λ_{max} defined as the maximum dynamic pressure at which the control system can suppress the LCO of nonlinear panel flutter. This quantity is governed by controller performance, piezoelectric saturation voltage, and LCO amplitude. To obtain conservative values for λ_{max}, the controller will be activated after the convergence of LCO. By the use of the LQG controller, λ_{max} was found to be 920, compared to 512 for the original panel and to 449 for the panel with embedded piezoelectric material and with no control applied. For the LQR/EKF nonlinear output controller, λ_{max} of 1750 was achieved, which is about a 90% performance improvement over the LQG due to the use of nonlinear state estimation. Note that, in practice, the panel flutter suppression performance will be further degraded due to sensor noise and system model uncertainty. Figure 7 shows a comparison between the performance of the LQG and LQR/EKF controllers in suppressing nonlinear panel flutter at $\alpha = 0$ deg and $\lambda = 1500$. It is shown that, unlike the LQR/EKF controller, the LQG controller cannot suppress the flutter LCO at $\lambda = 1500$.

The performance of the LQR/EKF controller for nonlinear panel flutter suppression under yawed flow is now considered. Three different configurations for piezoelectric placement are considered for comparison. The first and second configurations simply use the optimal placement determined at $\alpha = 0$ and 45 deg, respectively, whereas the third configuration uses the optimized piezoelectric over the range of 0 to 90 deg with four self-sensing actuators, as was shown in Fig. 6f. Figure 8 shows the achieved λ_{max} by the use of these three configurations for flow yaw angles changing from 0 to 90 deg.

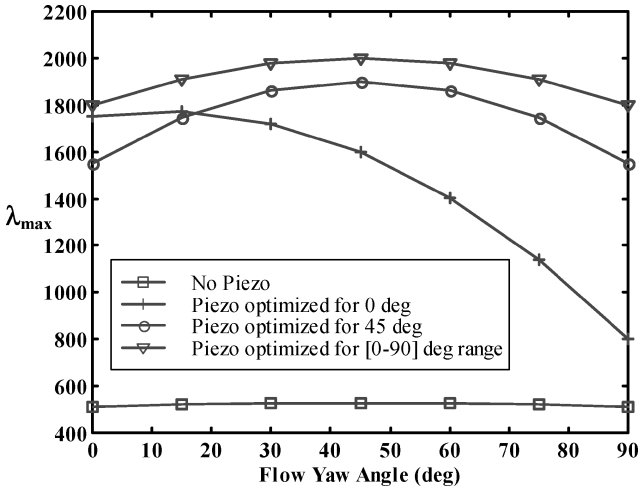

Fig. 8 Comparison of panel flutter suppression performance with LQR/EKF controller at different flow yaw angles and different piezoelectric placement configurations for a square isotropic panel.

Note that the piezoelectric optimized for 0-deg flow angle provides acceptable performance up to $\alpha = 45$ deg with $\lambda_{\max}/\lambda_{cr} = 3.03$ ($\lambda_{cr} = 512$), but that $\lambda_{\max}/\lambda_{cr}$ decreases to about 1.56 at $\alpha = 90$ deg compared to 3.41 at $\alpha = 0$ deg. Therefore, this configuration is not a good candidate for yaw angles from 0 to 90 deg. However, it provides acceptable performance from 0 to 45 deg and, consequently, from -45 to 45 deg due to the panel symmetry. The second configuration, piezoelectric optimized for $\alpha = 45$ deg, is shown to provide good flutter suppression performance over the entire range yaw angles from 0 to 90 deg. The best performance is achieved at $\alpha = 45$ deg with $\lambda_{\max}/\lambda_{cr} = 3.71$, whereas $\lambda_{\max}/\lambda_{cr} = 3.0$ at $\alpha = 0$ and 90 deg. The third configuration with four self-sensing piezoelectric actuators is shown to provide the best performance of all configurations with a minimum of $\lambda_{\max}/\lambda_{cr} = 3.52$ over the entire range of yaw angles. This is because the piezoelectric actuators cover the largest panel area, and, thus, the third configuration has the largest control power among the three configurations. Moreover, the advantage of the third configuration is that it provides control capabilities at negative flow yaw angles as compared with other configurations. Notice that the best performance is also achieved at $\alpha = 45$ deg. The reason is that the perpendicularly placed piezoelectric actuator patches provide the most rigid stiffness in the 45-deg direction.

2. Composite Panel

Nonlinear panel flutter suppression with yawed supersonic flow is also considered for a rectangular $38.1 \times 30.5 \times 0.12$ cm simply supported graphite/epoxy $[0/45/-45/90]_S$ panel. The addtion of too much piezoelectric material in this case will greatly change the panel characteristics because it replaces the 0-deg layer and, hence, changes the original panel directional properties. In addition, PZT5A mass density is very high compared to graphite/epoxy (about five times higher). To avoid adding too much piezoelectric material and changing the panel characteristics, piezoelectric material is only used as an actuator for this panel, and displacement sensors are used to provide output measurements for the estimation process. PZT5A actuators that have the thickness of 0.006 in. (0.015 cm) are embedded at the top and bottom layers, that is, replacing the 0-deg layer. The maximum actuator applied voltage is limited to 91.2 V in this case. The panel is modeled with a 10×10 MIN3 finite element mesh, and the nonlinear modal equations of motion are derived with the lowest 16 modes. The aerodynamic damping coefficient c_a is assumed to be 0.01, and the modal structural damping ratio equals 1%.

Similar to the isotropic panel case, the optimal actuator location is determined by division of the panel into 10×10 piezoelectric actuator elements at the top and bottom, then the use of an LQR state feedback gain matrix from these actuators to select the elements with the highest NFCG. Figure 9 shows an optimal piezoelectric actuator

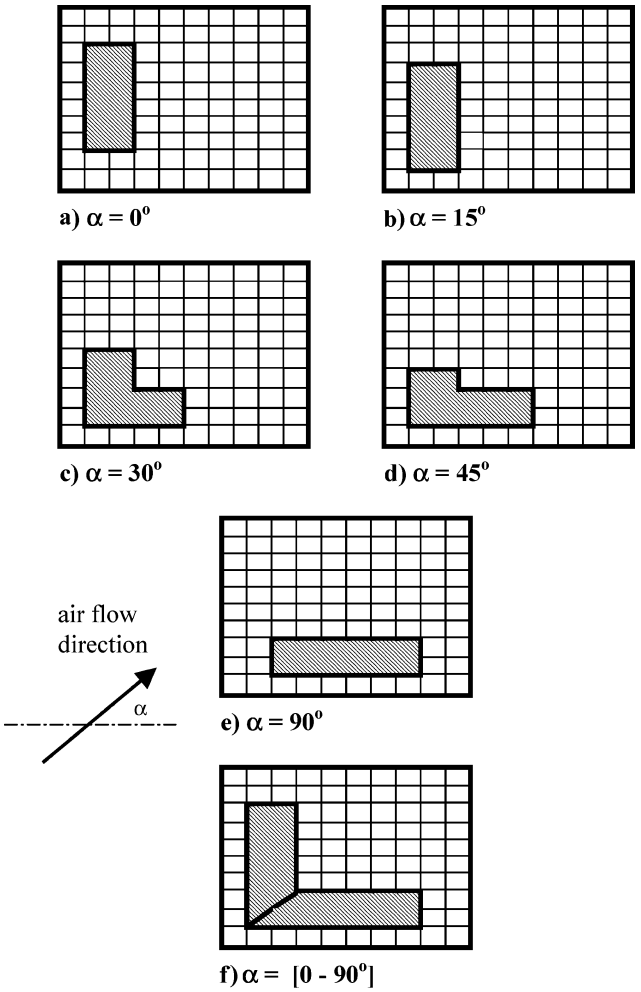

Fig. 9 Optimal piezoelectric actuator placement for [0/45/−45/90]$_S$ composite rectangular panel at different flow angles ranging from 0 to 90 deg.

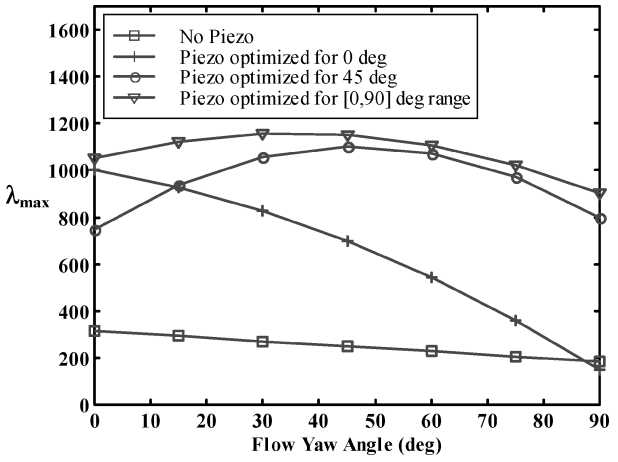

Fig. 10 Comparison of panel flutter suppression performance with LQR/EKF controller at different flow yaw angles and different piezoelectric actuator configurations for [0/45/−45/90]$_S$ rectangular composite panel.

using this method for different flow yaw angles at $\lambda = 800$. Given a yaw angle range from 0 to 90 deg, the shape of the piezoelectric actuator that cover all angles within this range is shown in Fig. 9f. The piezoelectric actuator shown in Fig. 9f is divided into two separate actuators, one perpendicular to the 0-deg flow direction and the other to the 90-deg flow direction. Three displacement sensors are used at the locations of ($3a/4$, $b/2$), ($3a/4$, $3b/4$), and ($a/2$, $3b/4$), corresponding to the approximate location of maximum deflection

for 0-, 45-, and 90-deg yaw angles, respectively. The performance of the LQR/EKF controller for nonlinear panel flutter suppression is studied with three different configurations for piezoelectric actuator placement; the optimal actuator for the case of $\alpha = 0$ deg, the optimal actuator for $\alpha = 45$ deg, and the optimized actuator over the range of 0–90 deg with two independent actuators. Figure 10 shows the achieved λ_{max} using these three configurations for flow yaw angles changing from 0 to 90 deg. The critical dynamic pressure changes largely with flow angle for the original panel with no piezoelectric actuators added, as was shown in Fig. 4b ($\lambda_{cr} = 315, 250$, and 185 for flow angles of 0, 45, and 90 deg, respectively). Figure 10 shows that the panel maximum flutter-free dynamic pressure can be increased to a minimum of 750 over all yaw angles from 0 to 90 deg by the use of the actuator optimized for 45 deg, or to a minimum of 900 by the use of the actuator optimized for all angles from 0 to 90 deg. This is compared to the minimum flutter-free dynamic pressure of 185 occurring at $\alpha = 90$ deg for the original uncontrolled panel.

V. Conclusions

A coupled structural–electrical time-domain modal finite element formulation for composite panels, with integrated piezoelectric sensors and actuators, is presented and used for nonlinear panel flutter suppression with yawed airflow. Finite element results for isotropic and composite panels showed that the flow yaw angle completely changes the shape of the panel limit-cycle deflection. Simulation studies were presented for the suppression of nonlinear panel flutter using both LQG and LQR/EKF controllers. The LQR/EKF nonlinear dynamic output controller was shown to have better performance than the linear LQG controller for nonlinear panel flutter suppression, with about a 3.5 times increase in the critical dynamic pressure as compared to only 1.8 times by the use of the LQG controller. This is because the LQG controller uses a linear Kalman filter to estimate the states of the nonlinear flutter dynamics. Nonlinear panel flutter suppression with flow yaw angle is considered with the LQR/EKF controller. The NFCG and the NKFEG methods are used to determine the optimal location of self-sensing piezoelectric actuators for different yaw angles. Optimal actuator and sensor location for a range of flow yaw angles is determined by grouping the optimal locations for different angles within the specified range. By the use of this method with four self-sensing actuators, the critical flutter boundary was increased about 3.5 times over the entire range of yaw angles from 0 to 360 deg for the square isotropic panel. For a rectangular graphite/epoxy composite panel with two independent piezoelectric actuators, the panel nondimensional critical flutter dynamic pressure is increased to a minimum of 900 over all yaw angles from 0 to 90 deg compared to 185 for the original uncontrolled panel. Future extensions of the current study will include the use of a more rigorous optimization method for optimal piezoelectric sensors and actuator location, such as genetic algorithms or gradient methods, and the investigation of robust and other nonlinear control methods.

References

[1]Mei, C., Abdel-Motagaly, K., and Chen, R., "Review of Nonlinear Panel Flutter at Supersonic and Hypersonic Speeds," *Applied Mechanics Reviews*, Vol. 52, No. 10, 1999, pp. 305–332.

[2]Friedmann, P., and Hanin, M., "Supersonic Nonlinear Flutter of Orthotropic or Isotropic Panels with Arbitrary Flow Direction," *Israel Journal of Technology*, Vol. 6, Nos. 1–2, 1968, pp. 46–57.

[3]Abdel-Motagaly, K., Chen, R., and Mei, C., "Nonlinear Flutter of Composite Panels Under Yawed Supersonic Flow Using Finite Elements," *AIAA Journal*, Vol. 37, No. 9, 1999, pp. 1025–1032.

[4]Tessler, A., and Hughes, T. J. R., "A Three-Node Mindlin Plate Element with Improved Transverse Shear," *Computer Methods in Applied Mechanics and Engineering*, Vol. 50, No. 1, 1985, pp. 71–91.

[5]Scott, R. C., and Weisshaar, T. A., "Controlling Panel Flutter Using Adaptive Materials," *Proceedings of the AIAA/ASME/ASCE/AHS/ASC 32nd Structures, Structural Dynamics, and Materials Conference*, AIAA, Washington, DC, 1991, pp. 2218–2229; also *Journal of Aircraft*, Vol. 31, No. 1, 1994, pp. 213–222.

[6]Surace, G., Ruotolo, R., and Di Terlizzi, D., "Active Control Laws for Panel Exposed to Supersonic Air Flow," *Proceedings of the 14th International Modal Analysis Conference*, Dearborn, MI, 1996, pp. 285–291.

[7]Frampton, K. D., Clark, R. L., and Dowell, E. H., "Active Control of Panel Flutter with Piezoelectric Transducers," *Journal of Aircraft*, Vol. 33, No. 4, 1996, pp. 768–774.

[8]Lai, Z., Xue, D. Y., Huang, J. K., and Mei, C., "Nonlinear Panel Flutter Suppression with Piezoelectric Actuation," *Journal of Intelligent Material Systems and Structures*, Vol. 6, No. 2, 1995, pp. 274–282.

[9]Zhou, R. C., Lai, Z., Xue, D. Y., Haung, J. K., and Mei, C., "Suppression of Nonlinear Panel Flutter with Piezoelectric Actuators Using Finite Element Methods," *AIAA Journal*, Vol. 33, No. 6, 1995, pp. 1098–1105.

[10]Zhou, R. C., Mei, C., and Haung, J. K., "Suppression of Nonlinear Panel Flutter at Supersonic Speeds and Elevated Temperatures," *AIAA Journal*, Vol. 34, No. 2, 1996, pp. 347–354.

[11]Dongi, F., Dinkler, D., and Kroplin, B., "Active Panel Flutter Suppression Using Self-Sensing Piezoactuators," *AIAA Journal*, Vol. 34, No. 6, 1996, pp. 1224–1230.

[12]Ho, M. T., Chen, R., and Chu, L. C., "Wind-Tunnel Testing of Panel Flutter Control Using Piezoelectric Actuation and Iterative Gain Tuning," *SPIE Conference on Smart Structures and Materials*, Society of Photo-Optical Instrumentation Engineers, Bellingham, WA, 1997, pp. 564–577.

[13]Kim, S. J., and Moon, S. H., "Comparison of Active and Passive Suppression of Nonlinear Panel Flutter Using Finite Element Method," *Proceedings of the AIAA/ASME/ASCE/AHS/ASC 41st Structures, Structural Dynamics, and Materials Conference*, AIAA, Reston, VA, 2000, pp. 691–699.

[14]Anderson, E. H., and Hagood, N. W., "Simultaneous Piezoelectric Sensing/Actuation: Analysis and Application to Controlled Structures," *Journal of Sound and Vibration*, Vol. 174, No. 5, 1994, pp. 617–639.

[15]Abdel-Motagaly, K., "Finite Element Analysis and Active Control for Nonlinear Flutter for Composite Panels Under Yawed Supersonic Flow," Ph.D. Dissertation, Aerospace Engineering Dept., Old Dominion Univ., Norfolk, VA, Dec. 2001.

[16]Abdel-Motagaly, K., Duan, B., and Mei, C., "Nonlinear Response of Composite Panels Under Combined Acoustic Excitation and Aerodynamic Pressure," *AIAA Journal*, Vol. 38, No. 9, 2000, pp. 1534–1542.

[17]Lewis, F. L., and Syrmos, V. L., *Optimal Control*, 2nd ed., Wiley, New York, 1995.

[18]Brown, R. G., and Hwang, P. Y. C., *Introduction to Random Signals and Applied Kalman Filtering*, 3rd ed., Wiley, New York, 1997.

[19]Sze, K. Y., and Yao, L. Q., "Modelling Smart Structures with Segmented Piezoelectric Sensors and Actuators," *Journal of Sound and Vibration*, Vol. 235, No. 3, 2000, pp. 495–520.

[20]Detwiler, D. T., Shen, M. H., and Venkayya, V. B., "Finite Element Analysis of Laminated Composite Structures Containing Distributed Piezoelectric Actuators and Sensors," *Finite Elements in Analysis and Design*, Vol. 20, No. 2, 1995, pp. 87–100.

[21]Dowell, E. H., "Nonlinear Oscillations of a Fluttering Plate I," *AIAA Journal*, Vol. 4, No. 7, 1966, pp. 1267–1275.

E. Livne
Associate Editor